Long-Term Nitrate Trajectories Vary by Season in Western European Catchments

Pia Ebeling[1], **Rémi Dupas[2]**, **Benjamin Abbott[3]**, **Rohini Kumar[4]**, **Sophie Ehrhardt[1]**, **Jan H. Fleckenstein[1,5]**, and **Andreas Musolff[1]**

[1]Department of Hydrogeology, Helmholtz Centre for Environmental Research-UFZ, Leipzig, Germany, [2]UMR SAS, INRAE, Institut Agro, Rennes, France, [3]Department of Plant and Wildlife Sciences, Brigham Young University, Provo, UT, USA, [4]Department of Computational Hydrosystems, Helmholtz Centre for Environmental Research-UFZ, Leipzig, Germany, [5]Bayreuth Center of Ecology and Environmental Research (BayCEER), University of Bayreuth, Bayreuth, Germany

Abstract Human alteration of nutrient cycles has caused persistent and widespread degradation of water quality around the globe. In many regions, including Western Europe, elevated nitrate (NO_3^-) concentration in surface waters contributes to eutrophication and noncompliance with environmental legislation. Discharge, NO_3^- concentrations and the vulnerability of the aquatic ecosystems to eutrophication often exhibit a distinct seasonality. Understanding spatial patterns and long-term trends in this seasonality is crucial to improve water quality management. Here, we hypothesized that NO_3^- concentrations during high-flow periods would respond faster to changes in nutrient inputs than low-flow concentrations because of greater connectivity of shallow diffuse NO_3^- sources with the river network. To test this hypothesis, we compiled long-term NO_3^- and discharge time series from 290 Western European catchments. To characterize the long-term trajectories of seasonal NO_3^- concentration, we propose a novel hysteresis approach comparing low- and high-flow NO_3^- concentration in the context of multi-decadal N input changes. We found synchronous winter maxima of NO_3^- and discharge in 84% of the study catchments. However, contrary to our hypothesis, there were surprisingly diverse long-term trajectories of seasonal NO_3^- concentration. Both clockwise (faster high-flow NO_3^- response) and counterclockwise hysteresis (faster low-flow NO_3^- response) occurred in similar proportions, potentially due to a high complexity in the underlying processes. Spatial variability of seasonality in NO_3^- concentration across the catchments was more pronounced and better predictable than its long-term variability. This work demonstrates the value of seasonal and inter-annual hydrochemical analysis and provides new tools for water quality monitoring and management.

Plain Language Summary Nitrogen is an essential element of all living organisms and has thus often been used excessively as fertilizer to secure food production. However, surface waters can suffer from elevated nutrients inputs, causing toxic algal blooms and impairing drinking water quality, especially during summer low flows. To manage water quality, it is crucial to understand these seasonal variations of nitrogen and discharge and the underlying processes. We used data from 290 catchments in France and Germany to characterize average seasonality patterns and their long-term evolution across the variety of landscapes and human influences. This allowed classifying catchment behavior and linking them to controls. As expected, both nitrogen and discharge peak during winter in most catchments (84%). However, there are well explainable deviations, for example, in mountainous regions. The long-term evolution of seasonality was more diverse than expected suggesting a complex interplay of various processes with the long input history from fertilization and wastewater being part of the controls. We found that the differences among catchments were greater than the long-term changes of seasonality within most catchments. By identifying catchment typologies, our study increases the understanding of nitrate seasonality patterns across a large extent and thus supports ecological water quality management.

1. Introduction

Many of the Earth's great biogeochemical cycles and nearly all of its ecosystems have been intensely influenced by human activities (Abbott et al., 2019; Vitousek et al., 1997). Some of the most dramatic changes have been associated with global nutrient cycles, with human inputs of reactive nitrogen (N) and phosphorus

(P) exceeding natural sources (Steffen et al., 2015). This global nutrient overload has triggered widespread eutrophication, causing toxic cyanobacterial blooms and expansive hypoxic "dead zones" in freshwater and coastal areas and impairing drinking water resources (Diaz & Rosenberg, 2008; Le Moal et al., 2019).

Diffuse agricultural sources are the dominant source of N (e.g., excessive fertilizer application and cultivation of N-fixing crops), but mitigation measures, such as reducing N input, often do not immediately lead to improved riverine water quality (Bouraoui & Grizzetti, 2011). Time lags between changes in N inputs and riverine N concentration can range from immediate to several decades due to legacy storage (e.g., Bouraoui & Grizzetti, 2011; Dupas et al., 2020; Ehrhardt et al., 2020; Meals et al., 2010). Factors that contribute to these time lags include fixation and long transit times in soils (Kumar et al., 2020; Sebilo et al., 2013; Van Meter et al., 2016), in vadose zone (Ascott et al., 2017) and in groundwater (Kolbe et al., 2016; Wang et al., 2016) affecting water quality trajectories of catchments (i.e., the long-term evolution of the catchment's response under changing external forcing) (Hamilton, 2012; Van Meter & Basu, 2015, 2017).

The nutrient-triggered eutrophication in freshwater resources shows a strongly seasonal behavior because its controlling factors light, temperature, and nutrient concentrations fluctuate intra-annually. As aquatic ecological communities are sensitive to those nutrient fluctuations, understanding these seasonal dynamics is necessary to assess and reduce the impact of nutrient pollution. Understanding the factors creating seasonal patterns of riverine N concentrations, discharge and thus flux and their trends could improve our ability to predict response times, long-term pollution trajectories, and priority locations for management interventions (Frei et al., 2020). This calls for large sample approaches to identify catchment typologies (i.e., archetypes) in seasonal water quantity and quality dynamics (e.g., Gupta et al., 2014; Newcomer et al., 2021) and to couple the seasonal time-scale with the long-term trajectories.

Patterns of seasonal N concentration variability are controlled by various interacting physical, climatic, biological, and anthropogenic factors, which vary among catchments. First, the relative contributions of point and diffuse sources can affect concentration seasonality (Van Meter et al., 2020). Point source dominance often leads to highest concentrations during low flow, while diffuse N sources are often exported with higher discharges (Abbott, Moatar, et al., 2018; Van Meter et al., 2020). Second, hydrological connectivity can variably activate heterogeneously distributed solute sources within the catchment as discharge fluctuates at seasonal or event scales (Aubert et al., 2013; Dupas et al., 2016; Seibert et al., 2009). For example, the vertical distribution of solutes in the subsurface can control the concentration-discharge (C-Q) relationship (Botter et al., 2020; Ebeling et al., 2021; Zhi & Li, 2020) at event, seasonal, and inter-annual scales (Minaudo et al., 2019; Moatar et al., 2017; Musolff et al., 2015; Zarnetske et al., 2018). Third, seasonal variations in hydroclimatic drivers and biogeochemical controls such as riparian or in-stream retention processes can create seasonal variations of riverine N concentrations (Casquin et al., 2020; Kumar et al., 2020; Lutz et al., 2020). For example, during summer low-flow conditions, biological N uptake and removal processes in the benthic and hyporheic zones can more strongly influence water column chemistry because residence times and temperature are higher (Moatar et al., 2017; Wollheim et al., 2017). Conversely, during high-flow periods, the larger flux of nutrients and the disturbance of aquatic nutrient uptake via scouring and sedimentation can result in minimal biological influence on stream chemistry (Blaszczak et al., 2019; Raymond et al., 2016). Among other things, this makes high-flow conditions the most important to nutrient flux, but summer low-flow conditions the most sensitive to eutrophication (e.g., Minaudo et al., 2020; Withers & Jarvie, 2008).

The seasonal variability of N concentrations can be characterized in terms of annual amplitude and timing of the minimum and maximum concentrations. Applied to multi-annual concentration time series this allows identification of long-term controls of seasonality, including strength and type of nutrient loading, which can change through time (Howden et al., 2010; Westphal et al., 2020). For example, decreases in point and diffuse source strength are expected to have greater influence on low-flow and high-flow concentrations, respectively (Abbott, Moatar, et al., 2018). More generally, decreases in point sources may have an immediate effect while diffuse sources are likely to show time lags as described above (Abbott, Moatar, et al., 2018; Westphal et al., 2020). This delayed response can differ between seasons (Ehrhardt et al., 2019; Van Meter & Basu, 2017) according to changes in hydrological connectivity and transit time, with a larger contribution from younger water during high flow periods (Benettin et al., 2017; Yang et al., 2018). Accordingly, Dupas et al. (2016), Ehrhardt et al. (2019) and Winter et al. (2020) demonstrated how changes in N

input loading to a catchment can alter long-term N export dynamics, seasonal amplitudes, and even reverse the seasonal timing, in some cases. In other cases, the timing of N seasonality was largely constant even under various concentration trends, potentially due to invariant vertical distributions of the nutrient source zones (Abbott, Moatar, et al., 2018; Dupas et al., 2018). Finally, changes in N seasonality can also be caused by changes in in-stream processes related to other factors, including P concentration (Bowes et al., 2011; Minaudo et al., 2015). As the inter-annual trajectories of low- and high-flow concentrations integrate the input history, retention and release processes at catchment scale, they can be a valuable characteristic and indicator of how catchments respond to changes in nutrient inputs.

Despite a growing body of work on N seasonality, the spatial variability of N concentration seasonality and its long-term trend are still poorly understood across catchments. In this context, we investigated spatio-temporal patterns of nitrate (NO_3^-) seasonality in 290 catchments from two unique datasets of long time series across France and Germany. These catchments cover a wide range of ecohydrological and land use conditions, allowing robust quantification of seasonality and trend parameters on decadal timescales. We hypothesized that in these Western European landscapes where NO_3^- sources are primarily diffuse, most catchments would show (a) a NO_3^- maximum during the winter high-flow season and (b) a faster response of high-flow NO_3^- concentrations to changes in loading compared to low flow because of shallower N sources being affected first and being activated during high flow. To test the hypotheses, we propose a hysteresis approach for long-term trends of NO_3^- seasonality using available low frequency data. We classified the catchments based on their long-term average NO_3^- and discharge seasonality as well as long-term trajectories of NO_3^- seasonality and assessed links between these metrics and potential controls such as mean precipitation and fraction of agricultural land use. This large sample approach allowed us to determine archetypes of spatiotemporal NO_3^- export patterns at continental scale and evaluate underlying processes.

2. Methods

2.1. Databases

We used long-term riverine NO_3^--N (NO_3-N, hereafter) concentration data and daily discharge (Q) data from stations in Germany and France to analyze spatiotemporal patterns of NO_3-N seasonality linking to export dynamics. From the original databases for Germany (Musolff, 2020; Musolff et al., 2020) and France (http://naiades.eaufrance.fr/; http://hydro.eaufrance.fr/; Dupas et al., 2019; Ehrhardt et al. (2021); Minaudo et al., 2019; Moatar et al., 2017) we selected stations based on the following criteria: (a) time series of NO_3-N covering at least 20 years, (b) with at least 150 NO_3-N samples, (c) a maximum sampling gap of 20% of the time series, (d) seasonal coverage, that is at least 10% of the data in each season (all possible quarterly divisions by months), and (e) available corresponding gauge with daily Q data. Discontinuous Q time series at 36 German stations were filled through the support of simulations from the grid-based distributed mesoscale hydrological model mHM (Kumar et al., 2013; Samaniego et al., 2010). Model results with a regression coefficient (R^2) greater than 0.6 with the observed Q were accepted. Next, we used a piece-wise linear regression to reduce bias in modeled Q data, used for gap-filling, following Ehrhardt et al. (2020). The criteria resulted in a set of 290 catchments (165 in France, 125 in Germany) with a median of 336 NO_3-N samples per station and 114,479 in total, which cover various temperate ecoregions, topographic, climatic and land cover settings (Figures 1 and S2). The median time series length was 32 years and the maximum length 46 years starting in 1969. The majority of time series started around 1980 and ended in 2014 or 2015.

We reconstructed daily concentrations (C) and flow-normalized concentrations (C_{FN}) using Weighted Regression on Time, Discharge and Season (WRTDS, Hirsch et al., 2010) as implemented in the R package *EGRET* (version 3.0.2, Hirsch & De Cicco, 2015). Flow-normalization estimates are calculated by averaging C estimates from all observed Q values of the specific day of the year throughout the time series. To focus on concentration trends independent of inter-annual discharge variations we use C_{FN} for our analysis. For data gaps of observed NO_3-N larger than two years, corresponding daily C_{FN} estimates were excluded due to high uncertainties, following Hirsch and De Cicco (2015). Observed and interpolated time series of the Wupper catchment are shown in Figures 2a–2c as an example.
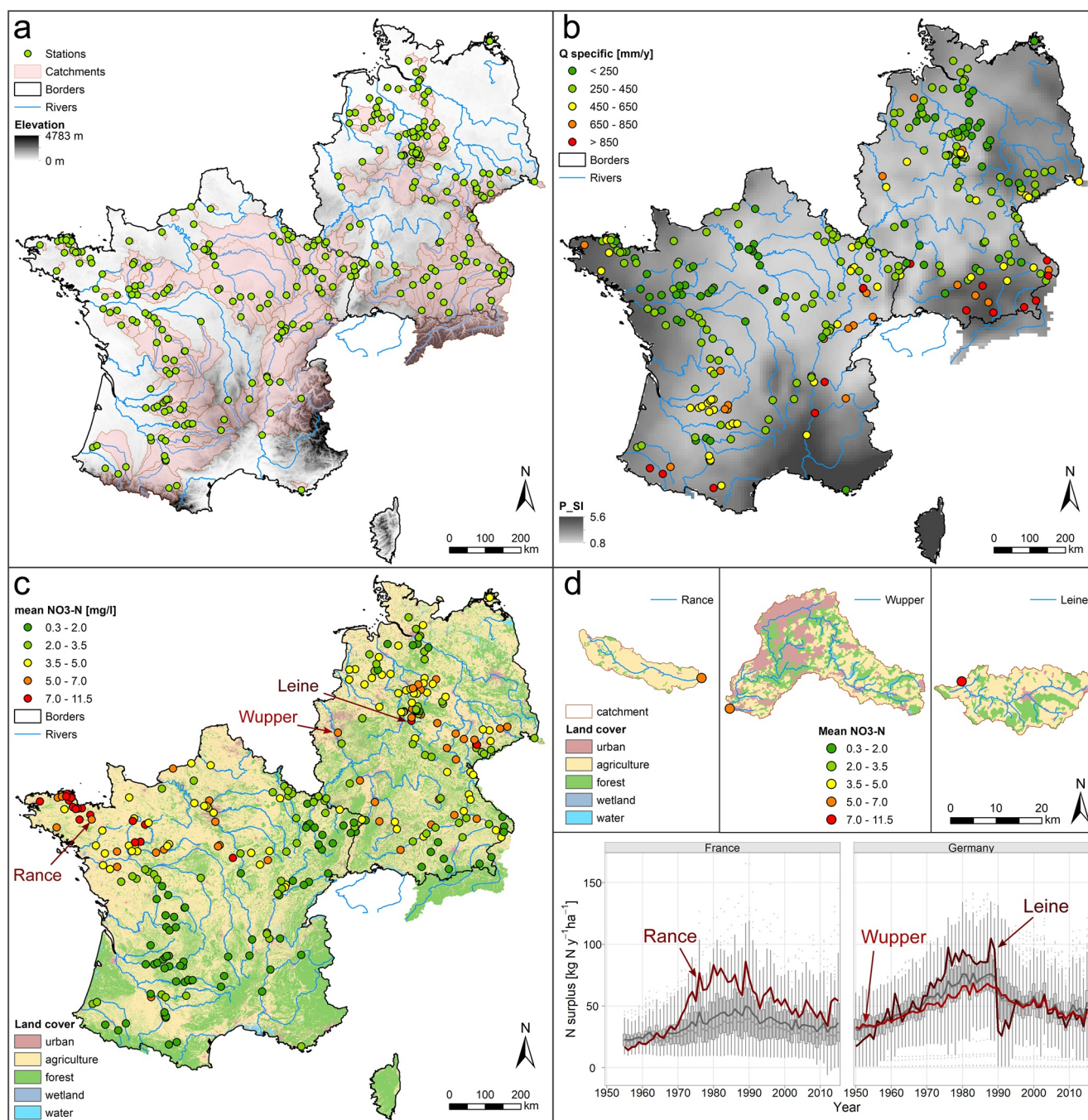
Figure 1. Map of the study area with (a) stations, catchments and elevation (EEA, 2013), (b) specific discharge and precipitation seasonality P_SI (Table S1, Cornes et al., 2018), (c) mean NO_3-N concentrations and land cover classes (CLC, 2006), (d) three selected catchments with mean NO_3-N, land cover, and N surplus time series. N surplus is the diffuse N input from agriculture, atmospheric deposition, and biological fixation in excess of N uptake by plants (for details refer to Ehrhardt et al. (2020) and Ebeling & Dupas, 2021, Table S1). In panel (d) boxplots represent annual N surplus averages of all catchments, gray lines represent mean values over all French and German study catchments, red lines represent single catchment time series.

2.2. Low- and High-Flow Seasons and Average Nitrate Seasonality

We determined the high-flow (HF) and low-flow (LF) seasons for each catchment by calculating the long-term average discharge for three consecutive months and defined the HF and LF seasons as the three wettest and driest months, respectively. Based on the timing of HF we classified the catchments into winter maximum (winMax, center of three wettest months within November–March) and spring or early summer
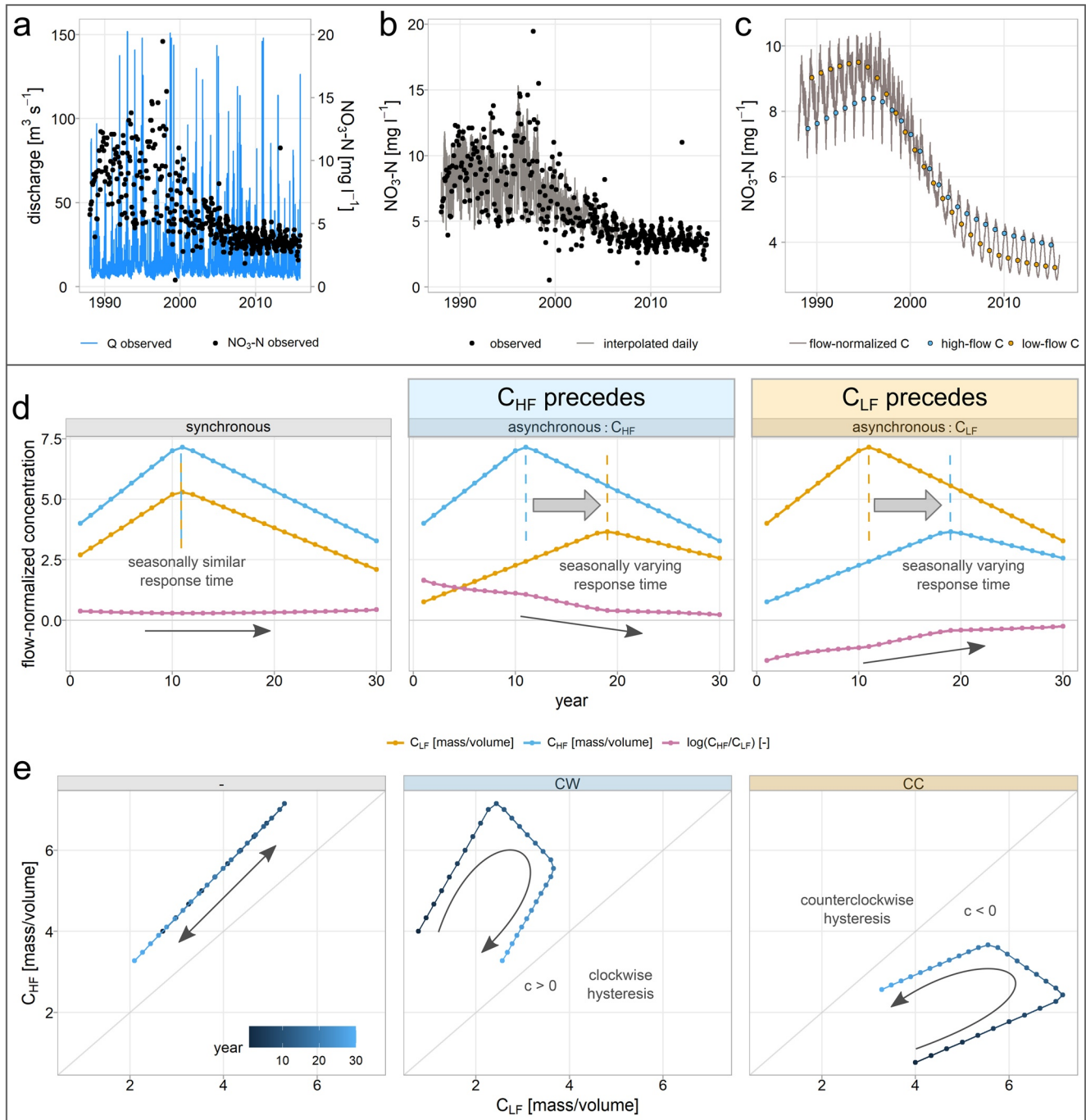
Figure 2. Conceptual framework of hysteresis between annual low-flow (C_{LF}) and high-flow (C_{HF}) concentrations. Upper box: Time series of the Wupper catchment for (a) observed daily discharge and weekly to monthly NO$_3$-N concentrations, (b) observed and daily WRTDS-interpolated NO$_3$-N concentrations, and (c) daily flow-normalized NO$_3$-N concentrations with annual averages during low-flow (C_{LF}) and high-flow (C_{HF}) periods. Lower box: Synthetic (d) time series of annual C_{LF} and C_{HF}, and the seasonal logarithmic ratio log(C_{HF}/C_{LF}), and (e) corresponding long-term hysteresis loops. The three distinct examples of long-term C-Q trajectories represent from left to right synchronous responses of C_{LF} and C_{HF}, asynchronous responses with C_{HF} preceding and asynchronous responses with C_{LF} preceding. The trajectories with a seasonally varying response times follow a hysteresis loop, while seasonally synchronous responses show no hysteretic behavior. Note that Figure 3 shows trajectories from three study catchments, including the Wupper catchment (as panels a–c), and Figure S1 presents more examples of possible trajectories.

Table 1
Metrics Used to Characterize Patterns of Q and NO₃-N Seasonality

Metric	Meaning	Calculation	Unit
seasQmax	Timing of Q seasonal maximum of long-term three months average (high-flow period)	Period of Q_{HF}	Classes: winMax, sprMax
rQseas	Long-term average of relative Q seasonal amplitude	$(Q_{HF} - Q_{LF})/mean(Q)$	-
C_{FN}	Flow-normalized (FN) concentrations	C_{FN} from WRTDS	mg NO₃-N l⁻¹
seasCmax	Timing of NO₃-N seasonal maximum of long-term months average	Period of maximum monthly NO₃-N C_{FN}	Classes: winMax, sumMax
C_{HF}, C_{LF}	Mean flow-normalized concentrations during HF and LF periods, calculated annually	$C_{HF} = mean(C_{FN}(HF))$ $C_{LF} = mean(C_{FN}(LF))$	mg NO₃-N l⁻¹
log(C_{HF}/C_{LF})	Logarithmic seasonal ratio, calculated annually	$log(C_{HF}/C_{LF})$	-
rCseas	Mean relative NO₃-N seasonal amplitude between HF and LF seasons	$mean(abs(C_{HF} - C_{LF}))/mean(C_{FN})$	-
c	Hysteresis between C_{LF} and C_{HF}	See Equation 1,	Classes:
		$c < 0$	CC,
		$c > 0$	CW,
		$c \approx 0$	n.s.

maximum (sprMax, April–July; metric seasQmax, see Table 1). The LF season was calculated but not used for an additional classification of average Q seasonality. Similarly, we determined the average seasonal concentration pattern at each station. We calculated the maximum monthly averages of C_{FN} to classify the catchments into the ones with their intra-annual maximum during winter (winMax, November–March) and summer (sumMax, April–October; metric seasCmax, see Table 1). The combination of both classifications yields the long-term average *C-Q* seasonality.

2.3. Hysteresis in Multi-Annual Time Series of Low- and High-Flow Concentrations

We calculated mean C_{FN} during LF (C_{LF}) and HF (C_{HF}) periods (see Section 3.2) for each hydrological year (November–October) and catchment from the WRTDS-interpolated daily C_{FN} time series (Section 2.1, see Figure 2c as example). We only calculated these values with at least 80% daily data coverage over the corresponding time period. As a metric of the strength of *C-Q* seasonality within each year, we calculated the annual seasonal ratio in logarithmic form log(C_{HF}/C_{LF}). Example trajectories of C_{LF}, C_{HF} and log(C_{HF}/C_{LF}) are shown in Figure 2d.

To identify and characterize the seasonally asynchronous (i.e., phase/time shift between peaks) responses to changes in inputs, we plotted the time series of annual mean C_{LF} and C_{HF} against each other and applied a hysteresis approach (Figure 2e). Accordingly, the hysteresis captures decadal trajectories of the seasonality represented by time series of annual average low- and high-flow concentrations. Systematic changes in the trajectories are considered to be linked to changes in point and diffuse source inputs with mainly increasing inputs before 1990s and decreases mainly after 1990s (Figure 1d) in response to European regulations as drivers (EEC, 1991a, 1991b). If C_{HF} (*y*-axis) responds faster than C_{LF} (*x*-axis) hysteresis becomes clockwise (CW), while if C_{LF} responds faster than C_{HF} hysteresis will be counter-clockwise (CC). If C_{HF} and C_{LF} respond simultaneously, no significant hysteresis loop is observed (n.s.). We used a hysteresis method based on the derivative of the *X* variable (d*X*)C_{LF} (Krueger et al., 2009; Minaudo et al., 2019). Its advantage for long-term water quality trajectories is that it also works for incomplete hysteresis loops. Incomplete loops are common for example, if (a) sampled time series are too short to cover the complete loop or (b) catchments do not return to their original state due to continued differences in the pressures or changes in their functioning. To this end, we fit the following nonlinear model using the R package *minpack.lm* (version 1.2–1).

$$C_{HF}'(t) = d + mC_{LF}'(t) + c\frac{dC_{LF}'(t)}{dt} \tag{1}$$

where t represents the time in years, d is the intercept, m is the slope between C_{HF}' and C_{LF}', and c is the hysteresis coefficient describing the direction and width of the hysteresis ($c < 0$ corresponds to a CC, $c > 0$ to CW, and $c \approx 0$ to a non-significant hysteresis based on a confidence level of 95%). Prior to fitting, we linearly scaled C_{LF} and C_{HF} to vary between 0 and 1 (C_{LF}' and C_{HF}') to make the hysteresis coefficient c of different catchments comparable independent of differences in concentration (Lloyd et al., 2016).

Variations in seasonal response times cause trends in concentration seasonality and export dynamics, that is here $\log(C_{HF}/C_{LF})$ (Figure 2a). Therefore, we use the Mann-Kendall test (R package *Kendall*, version 2.2) and Sen's slope (Sen, 1968) (R package *trend*, version 1.1.2) to detect and quantify monotonic trends in the logarithmic seasonal ratio. Missing annual values at 40 stations were filled by linear interpolation (on average 4.25 interpolated values, maximum eight), for example caused by large gaps in NO_3^--N samples (see Section 2.1).The ratio C_{HF}/C_{LF} is linked to the slope b of the $\log C$-$\log Q$ regression and is thus another metric of C-Q relationships. The slope b is a widely used metric to characterize solute and particulate export dynamics in terms of C-Q relationships (Godsey et al., 2009).

$$C = aQ^b \tag{2}$$

$$\log(C) = a + b\log(Q) \tag{3}$$

with a being the intercept and b the slope of the $\log C$-$\log Q$ regression. If we assume a mean Q for HF (Q_{HF}) and another for LF (Q_{LF}) periods, the quotient becomes constant and b dependent on the logarithmic seasonal C_{FN} ratio.

$$b = \frac{\mathrm{dlog}(C)}{\mathrm{dlog}(Q)} = \frac{\log\left(\dfrac{C_{HF}}{C_{LF}}\right)}{\log\left(\dfrac{Q_{HF}}{Q_{LF}}\right)} \tag{4}$$

If the ratio of Q_{HF}/Q_{LF} equals Euler's number ($\sim$2.718), b becomes equal to $\log(C_{HF}/C_{LF})$. Generally speaking, b behaves proportional to the logarithmic seasonal C_{FN} ratio normalized by the logarithmic seasonal ratio of discharge $\log(Q_{HF}/Q_{LF})$. Though of course, slope b would be more scattered when considering the actual inter-annual Q variability instead of the long-term mean.

Additionally, we assessed and compared both the spatial variability and the long-term temporal variability of NO_3-N seasonality. The spatial variability was determined for each year as the standard deviation of annual $\log(C_{HF}/C_{LF})$ across all stations. The temporal variability was calculated for each station as the standard deviation of annual $\log(C_{HF}/C_{LF})$ over the complete time series including the long-term trends in the seasonality trajectories.

2.4. Linking Metrics and Catchment Characteristics

We tested for relationships between the two classifications of long-term average C-Q seasonality and its trajectory (hysteresis) and catchment descriptors to examine our hypothesis about dominant controls. For the descriptors we used the data sets published and described in Ebeling et al. (2021), Ebeling (2021) and extended to include French catchments in Ebeling and Dupas (2021). The descriptors characterize the hydroclimatic settings, topography, land cover, soil properties, geology, and point and diffuse N sources of the study catchments (Figure S2, Table S1).

The analyzed metrics are partly categorical and partly continuous (Table 1). To test for significant differences among the different classes of long-term average C-Q seasonality and hysteresis trajectories, we used the non-parametric Wilcoxon test for comparing two classes and otherwise the Kruskal-Wallis test. A random forest (RF) classification model was trained for the two significant hysteresis classes (CC and CW) to investigate the joint predictive power of the descriptors while accounting for collinearities (see Figure S3). We used three times repeated tenfold cross-validation to estimate the mean model performance. Subsequently, permutation allows quantifying variable importance and thus identifying the dominant descriptors from the trained RF model. We used the importance permutation by Altmann et al. (2010) to identify significant descriptors from a first RF model using all descriptors (significance level 5%; Table S1), which then served to train a second RF model. We used the R package *mlr3* (version 0.9.0, Lang et al., 2019) to train the RF model and *ranger* (version 0.12.1, Wright & Ziegler, 2017) for permutation variable importance. Spearman

Table 2
Summary Statistics of Calculated Metrics of All Catchments (n = 290) From Observations and the WRTDS Models:
Median and Interquartile Range (IQR) and the Number of Catchments (n) With Positive (+), Negative (−) or Non-
Significant (n.s.) Monotonic Mann-Kendall (MK) Trend

		Specific Q	Rel. seasonal Q amplitude rQseas	Mean NO_3-N C_{FN}	Mean NO_3-N C_{LF}	Mean NO_3-N C_{HF}	Rel. seasonal NO_3-N amplitude rCseas	Mean $\log(C_{HF}/C_{LF})$
		mm y^{-1}	-	mg N l^{-1}	mg N l^{-1}	mg N l^{-1}	-	-
Median		340	1.18	3.23	2.51	3.92	0.37	0.33
IQR		254	0.55	2.95	2.46	3.68	0.45	0.53
n MK trend	+	2		92				124
	−	32		151				95
	n.s.	256		47				71

Note. Q—discharge, FN—flow normalized, LF—low flow, HF—high flow. The Q values used for these statistics was the same time period used for the WRTDS model, that is the overlapping period of NO_3-N and Q time series.

rank correlations served to identify relevant descriptors for the continuous metrics of average Q seasonality (rQseas) and NO_3-N seasonality (mean $\log(C_{HF}/C_{LF})$).

3. Results

3.1. Spatial Patterns of Long-Term Average Discharge and Nitrate Seasonality

The highest specific Q was observed in mountainous catchments (e.g., the Alps) with values up to 1,670 mm y^{-1} (median 340 mm y^{-1} among the study catchments) while lowest specific Q was 63 mm y^{-1}. The relative seasonal Q amplitude (rQseas) was highest in northwestern France (max 2.50) and lowest mostly in southeastern Germany (min 0.11) with a median of 1.18 (see Figure S4). A summary of calculated metrics across the study catchments is presented in Table 2.

Across the catchments, we found a dominance of winter maxima in Q (90.3%) and in flow-normalized NO_3-N concentrations (91.0%) (Figure 3) with occurrence of both in 83.8% of the catchments. The 9.7% of catchments with spring and early summer maxima of Q (sprMax) were apparent in mountainous areas (Figure 3a). The 9.0% of catchments with summer maxima of NO_3-N (sumMax) were observed mainly in northwestern and southern France (Figure 3a). In southern France, these summer NO_3-N maxima coincided with Q minima, while NO_3-N minima coincided with the Q maxima in spring. Catchments with spring maxima of Q in southeastern Germany have lowest Q during autumn or winter, which coincided with maxima in NO_3-N. Figure S5 shows these synchronous and asynchronous long-term average seasonal C and Q variations of the four combined C-Q seasonality classes.

Catchments with the largest positive average seasonal ratios ($\log(C_{HF}/C_{LF})$) were found in western France, northern Germany and northeastern France (Figure 3a). On the other hand, catchments with average $\log(C_{HF}/C_{LF}) < 0$ were observed mainly in southern Germany, southern and western France. The spatial variability of the NO_3-N seasonality among the catchments (standard deviations of $\log(C_{HF}/C_{LF})$ over all stations for each year) ranged from 0.42 to 0.64 with a median of 0.47 and an interquartile range of 0.04.

3.2. Long-Term Trajectories of Nitrate Seasonality

We exemplarily visualized the seasonal NO_3-N trajectories of three representative catchments namely the Wupper as an urban and the Leine and the Rance as agricultural rural catchments (Figures 1d and 3c). The Wupper catchment (605.9 km^2) has the highest fraction of artificial surfaces (31%), population density, and load by point sources and ranks under the top three for the fraction of point source loads from the total N input loads (86%) among the studied catchments. The HF season was determined for winter (December–February), LF for summer (May–July). The C_{LF} were higher than the C_{HF} in the beginning, but with C_{LF} decreased from 1994 until $C_{LF} < C_{HF}$ from 1998, indicating a switch in the seasonal timing. The peak
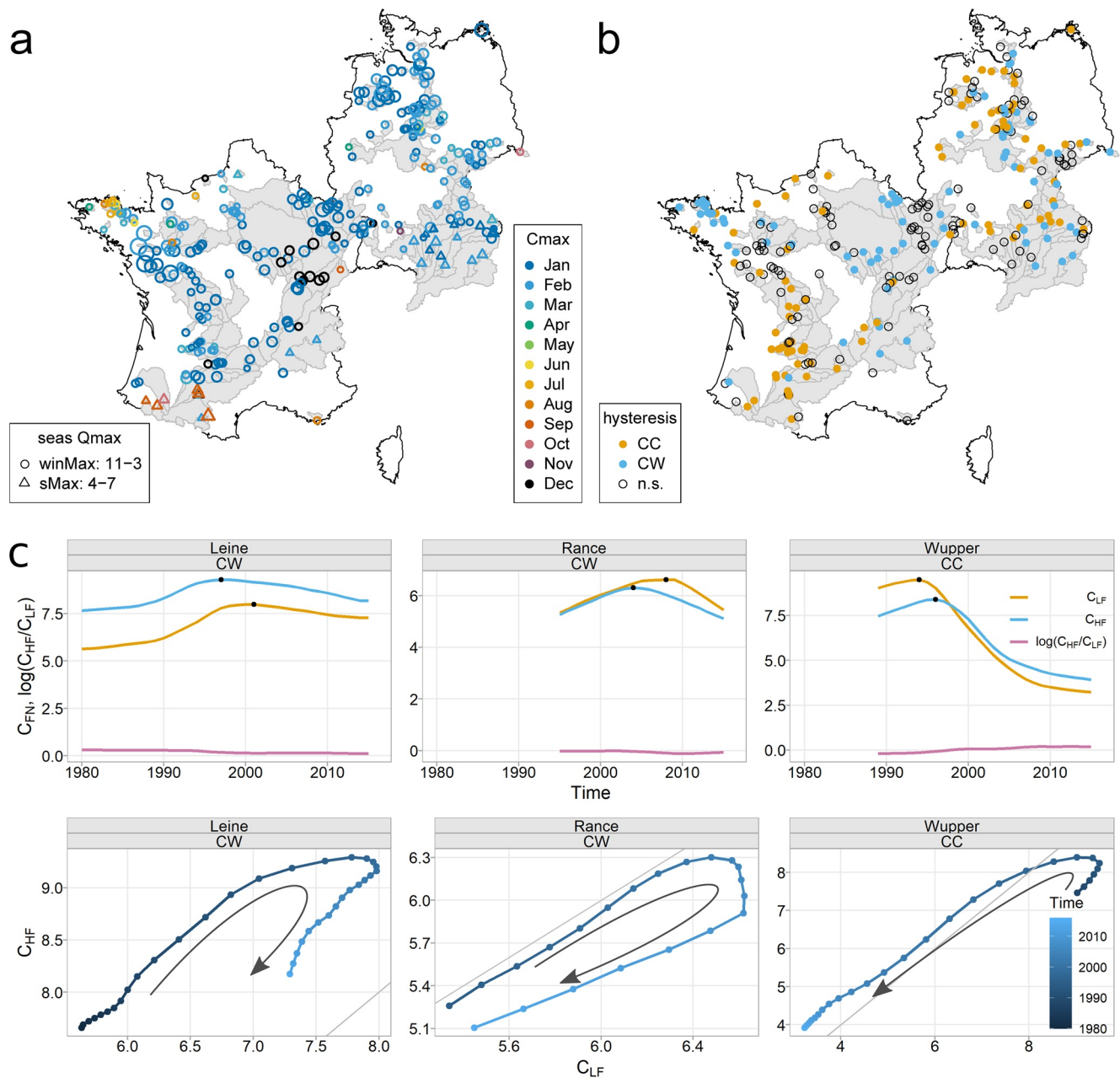
Figure 3. Spatial patterns of (a) average Q and NO_3-N seasonality, color—month with maximum long-term averages of flow normalized concentrations (C_{FN}), shape—timing of maximum average Q (seasQmax), size—absolute average seasonal ratio in log space $\log(C_{HF}/C_{LF})$, and (b) classes of hysteresis between C_{LF} and C_{HF} trajectories, color—hysteresis class, and (c) seasonal NO_3-N concentration trajectories during low-flow (C_{LF}) and high-flow (C_{HF}) periods and the corresponding hysteresis patterns of the three catchments Leine, Range and Wupper, black dots mark the peak concentrations. CC—counterclockwise hysteresis, CW—clockwise hysteresis, Time in years, concentrations in mg NO_3-N l^{-1}.

in C_{LF} is two years before the peak in C_{HF}, which creates a counterclockwise hysteresis. Accordingly, the seasonal ratio $\log(C_{HF}/C_{LF})$ follows a positive trend from a seasonal dilution ($\log(C_{HF}/C_{LF}) < 0$) to enrichment ($\log(C_{HF}/C_{LF}) > 0$) pattern. On the other hand, the two catchments with clockwise hysteresis, Leine (317.4 km²) and Rance (142.6 km²), are selected from catchments with high agricultural impact (65%–90%), strong change in diffuse agricultural N input from before to after 1990 (Figure 1d, and small urban areas (2.6%–6.8%) as well as low fraction of point sources from total N input (below 10%)). The HF season in both catchments is in winter (Leine: January–March; Rance: December–February) and LF season in summer to fall (Leine: August–October; Rance: July–September). In the Leine catchment, C_{HF} peaks in 1997 four years

before C_{LF}. In the Rance, C_{HF} peaks in 2004 also four years before C_{LF} with C_{LF} being slightly higher than C_{HF}. Both catchments have a negative trend in the seasonal ratio $\log(C_{HF}/C_{LF})$, which for the Leine means a trend from enrichment to a more neutral export pattern and a decrease in seasonal amplitude and for the Rance from neutral to dilution with an increase in the absolute seasonal amplitude between C_{LF} and C_{HF}.

Although the input trajectories of N surplus are relatively synchronous among the catchments (including the three example catchments) following the EU and national legislation (Figure 1d), the seasonal NO_3-N trajectories observed in the streams differ more prominently among the catchments (Figure S6). Exceptions to this generally synchronous variation in N surplus can be found in East German catchments with a drastic drop in 1990 after the German reunification, including the upper Leine catchment.

For all study catchments, counterclockwise and clockwise hysteresis occurred both in similar proportions ($n = 87$ CC, $n = 85$ CW, about 30% each), while the nonsignificant hysteresis class occurred slightly more often ($n = 116$ n.s., 40%). The fitted hysteresis models had a median performance of $R^2 = 0.84$ and a $R^2 > 0.6$ in 73.8% of the catchments. A spatial organization of the hysteresis patterns was apparent with clusters being more pronounced in France (Figure 3b): counterclockwise hysteresis dominated in central, southern and southwestern France and northern Germany, whereas clockwise hysteresis dominated in Brittany and northeastern France including the Seine catchment and southeastern Germany. In the majority of the catchments (80.3%, $n = 233$) the timing of seasonal C_{FN} maxima and minima remained constant throughout the time series, whereas in 19.7% ($n = 57$) it switched between HF and LF periods (e.g., in the Wupper catchment, Figure 3c). The majority of the switching catchments (54%, $n = 32$) changed once from a seasonality with $C_{LF} > C_{HF}$ to $C_{LF} < C_{HF}$ with the median switch in the year 1991. Most of these catchments had counterclockwise hysteresis patterns (63%, $n = 20$). Some of those catchments (32%, $n = 18$) changed the seasonal timing of concentration maxima more than once.

The C_{LF}-C_{HF}-hysteresis patterns were connected to long-term trends in the annual seasonal ratios $\log(C_{HF}/C_{LF})$ (significance level 5%, Figure S6): 60.9% of the counterclockwise catchments had a positive trend in $\log(C_{HF}/C_{LF})$ and 49.4% of clockwise catchments had a negative trend in $\log(C_{HF}/C_{LF})$. The nonsignificant hysteresis was mostly linked to a significant increase in the seasonal ratio (43.0%). The different trajectories imply a long-term temporal variability in the NO_3-N seasonality. The temporal variability of $\log(C_{HF}/C_{LF})$ at each station varied between 0.01 and 0.54 with a median of 0.09 and an interquartile range of 0.09.

3.3. Linking Seasonality Metrics and Catchment Characteristics

First, we linked the classifications of long-term average C-Q seasonality and the long-term trajectories to each other: The dominant class with NO_3-N and Q winter maxima had similar proportions of all three hysteresis classes (25.9% for CW, 32.1% for CC and 42.0% for n.s.). The two asynchronous NO_3-N and Q classes with Q winter and NO_3-N summer maxima or Q spring/summer and NO_3-N winter maxima both had higher proportions of clockwise hysteresis (63.2% and 47.6% respectively) compared to counterclockwise (10.5% and 14.3%) hysteresis. On the other hand, the asynchronous C-Q seasonality class in southern France with Q spring/summer and NO_3-N summer maxima (LF period) had mostly counterclockwise (57.1%) and no clockwise (0%) hysteresis.

The timing of Q seasonality linked to elevation (Figure 4a) and related hydroclimatic descriptors, that is catchments with Q spring/summer maxima had significantly higher mean elevations, precipitation and specific discharge and lower mean temperatures. The relative Q amplitude (rQseas) also correlated with the hydroclimatic drivers, especially the summer to winter precipitation P_SIsw ($r = -0.63$, Spearman rank, Figure S3) and mean temperature ($r = 0.63$).

The combined timing of NO_3-N and Q seasonal maxima (Figure 4a) linked to more characteristics in addition to the controls of only Q seasonality. Compared to catchments with maximum NO_3-N concentrations in summer, catchments with winter maxima of NO_3-N tended to be more abundant in catchments with higher ratios of summer to winter precipitation (P_SIsw) and discharge (Q_seasR, not shown) and lower Q seasonality (rQseas), although the class of concurrent NO_3-N and Q winter maxima contained many catchments with equilibrated summer to winter precipitation (P_SIsw~1) and smaller precipitation seasonality (P_SI, not shown). Summer maxima in NO_3-N emerged in catchments with consistently lower summer to winter precipitation (P_SIsw < 1, with only one exception) and lower depths to bedrock (dtb). We also found a link
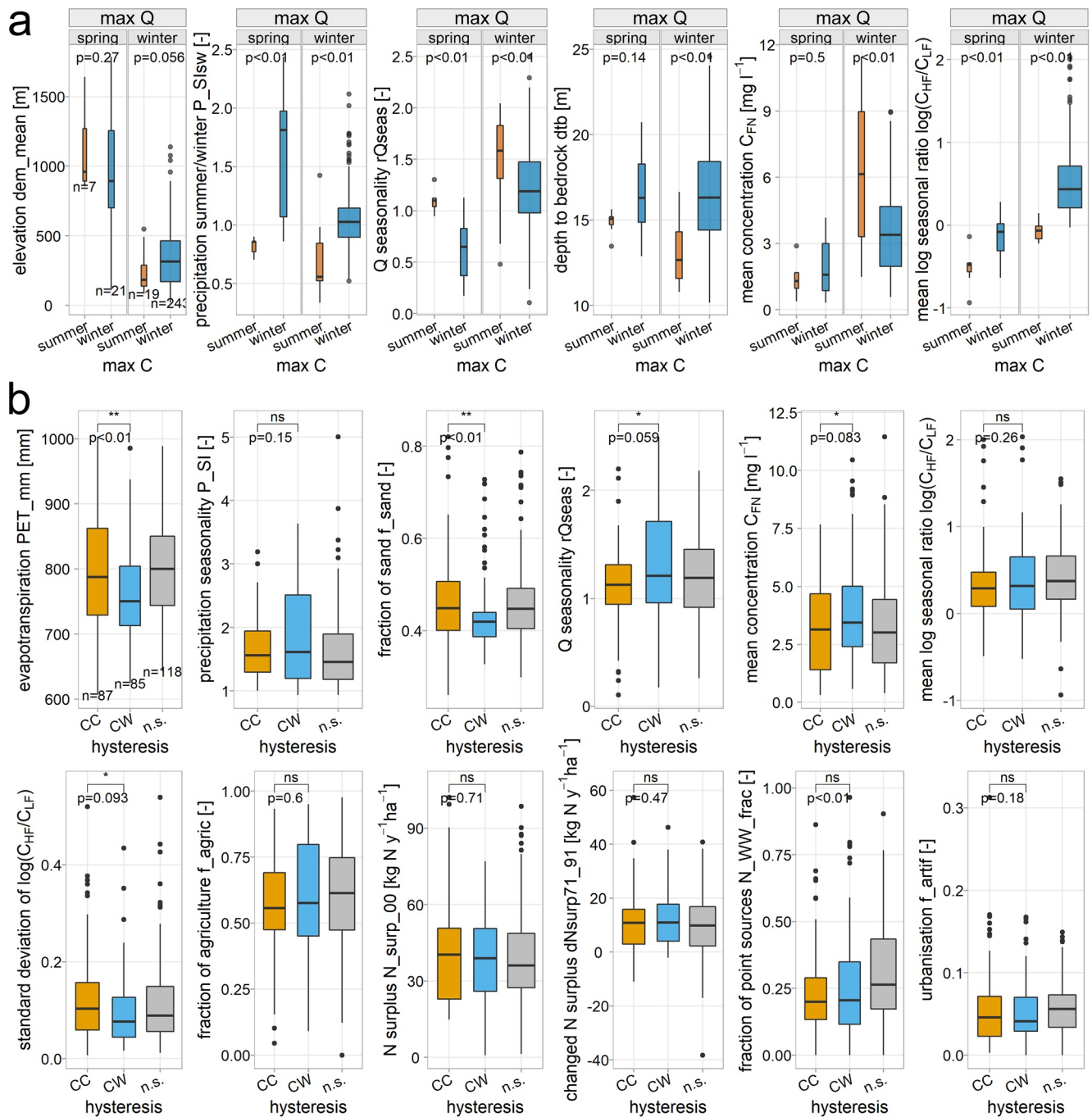
Figure 4. Controls of (a) long-term average NO$_3$-N and Q seasonality and (b) hysteresis classes (n.s. nonsignificant, CC counterclockwise and CW clockwise hysteresis). In panel (a), the classes of maximum NO$_3$-N concentrations are shown separately for each class of the timing of maximum Q (high flow) to distinguish the controls of the different identified combinations of C and Q seasonality. Number of samples (n) per group is given in the first subplot. The p values from Kruskal-Wallis tests for nonparametric comparisons of means for multiple groups and the significance levels from Wilcoxon rank sum tests for the pairwise comparison between CC and CW hysteresis are written above the boxplots (ns - $p > 0.05$, * - $p \leq 0.05$, ** - $p \leq 0.01$). For details on the variables refer to the text, Tables 1 and S1.

of average NO$_3$-N concentration to long-term average C-Q seasonality: The mean C_{FN} was lowest for the classes with Q spring/summer maxima and highest for Q winter maxima with NO$_3$-N summer maxima (especially in the Armorican Massif). The major class of concurrent NO$_3$-N and Q winter maxima has medium mean C_{FN} values but also a high range. . As expected from the methods, the classes were clearly linked to the

strength of the NO_3-N-Q seasonality, quantified by the mean seasonal ratio $\log(C_{HF}/C_{LF})$, with the class of concurrent NO_3-N and Q winter maxima showing mostly positive and the other classes negative values. The mean ratio $\log(C_{HF}/C_{LF})$ was correlated to topographical and hydroclimatic descriptors (slo.mean $r = -0.45$, twi.mean $r = 0.43$, AI $r = 0.41$, specific Q $r = -0.39$) and land use (f_agric $r = 0.39$). Note that the descriptors also correlate with each other (Figure S3).

The RF model for the two significant hysteresis classes reached only a mean accuracy of 0.69 ± 0.12 from cross-validation (compared to 0.5 for random guess). The descriptor relative Q seasonality (rQseas) ranked highest in the feature importance, followed by evapotranspiration (PET_mm), mean C_{FN}, precipitation seasonality (P_SI), ratio of summer to winter discharge (Q_seasR) and fraction of sand (f_sand), although they showed overall relatively low variable importances (Figure S7). Expected links to descriptors of N loading were not found dominant: although N surplus descriptors were significant in the RF model, they only ranked 8th or lower. As shown in Figure 4b, the clockwise hysteresis was mostly noticed in catchments with higher Q and precipitation seasonality (rQseas and P_SI), and mean C_{FN} and lower evapotranspiration (PET_mm), fraction of sand (f_sand), and temporal variability in NO_3-N seasonality (standard deviation of $\log(C_{HF}/C_{LF})$). The clockwise catchments covered a large variability in the fraction of agriculture, N surplus, the difference in N surplus before and after 1990 (dNsurp71_91), the fraction of point source loads (N_WW_frac) and artificial surfaces (f_artif). The nonsignificant hysteresis class contained more catchments with higher fractions of point source loads, albeit with a large variability of values.

4. Discussion

4.1. Spatial Patterns and Controls of Long-Term Average Nitrate and Discharge Seasonality

The long-term average NO_3-N seasonality was linked to average seasonality of Q in combination with climate, topography and geology. Accordingly, we established distinct archetypal patterns across the large range of catchments and provide possible links to the underlying catchment characteristics. The different timing of Q seasonality (seasQmax) across the catchments was controlled by topography and related hydroclimatic variables. This agrees with Kuentz et al. (2017), who found climate was the main driver for several flow characteristics at the European scale, and Gnann et al. (2020), who found catchment aridity to control the timing and magnitude of Q seasonality relative to climate seasonality. The dominance of Q winter maxima (90.3%) and summer low flow (Figure S5) suggests that the seasonal cycle of evapotranspiration strongly affects the Q cycle in the study region. Precipitation seasonality (P_SIsw) with relatively high winter precipitation (as prevalent in France) can add to this pattern, especially in northwestern France with the lowest ratios of summer to winter precipitation (P_SIsw) and relatively low annual evapotranspiration and aridity. In that region, the opposing seasonal precipitation and evapotranspiration cycles in a moist climate lead to strong seasonal Q patterns (rQseas) and short hydrological transport times (Gnann et al., 2020; Kumar et al., 2020), which might also be enhanced by shallow aquifers with shallow depths to bedrock (dtb). The Q maximum is shifted to spring or summer in fewer catchments (9.7%), where winter precipitation is likely retained as snow-pack and discharged with higher temperatures during thawing period. Here, this effect seems to exceed the evapotranspiration control. The spatial patterns of high-flow seasonality (Figures 3a and S4) largely agree with the flood timing reported across the study region, especially the geographical differences between the mountainous, snow-impacted catchments (in the Alps and Pyrenees) and others (Berghuijs et al., 2019; Blöschl et al., 2017).

In combination with the NO_3-N seasonality, we found three archetypal patterns of long-term average C-Q seasonality with different controls and underlying processes:

1. Both NO_3-N and Q have a winter maximum (83.8% of the catchments) and vary mostly synchronously (Figures 3a and S5), which indicates prevalent enrichment patterns (transport limitation) and NO_3-N mobilization processes at a seasonal scale (Minaudo et al., 2019). This supports our first hypothesis that overall synchronous NO_3-N and Q seasonality dominate. The dominance of NO_3-N and Q winter maxima and C-Q enrichment patterns agrees with previous research on temperate catchments (Ebeling et al., 2021; Minaudo et al., 2015; Moatar et al., 2017; Musolff et al., 2015; Zhi & Li, 2020). Moreover, the spatial patterns of the strength of nitrate-discharge seasonality, represented by the average seasonal ratio $\log(C_{HF}/C_{LF})$, are also in line with a previous study of Germany-wide C-Q relationships showing

strong enrichment patterns in northern Germany and less pronounced enrichment or neutral patterns in central-eastern Germany (Ebeling et al., 2021). This supports that the seasonal ratio is comparable to the widely used slope b for inter-annual *C-Q* relationships (see Equation 4). This is plausible as seasonal NO_3-N variations exceed storm-event induced variations, when considering rather large catchments are usually monitored at low (typically monthly) frequency (Minaudo et al., 2019). Furthermore, our analysis showed the dominant control of topography, climate and land use in shaping the spatial variability of the seasonal ratio, with a tendency of higher ratios in agricultural lowland catchments. With dominant diffuse N sources, a mechanism leading to this synchronous archetype can be variable discharge generating zones, where shallow N sources are activated by younger water dominating during HF and lack of connectivity of sources along with longer reaction times (potentially higher removal) for longer flow paths dominates during LF (Benettin et al., 2020; Musolff et al., 2016; Yang et al., 2018; Zhi & Li, 2020). This interpretation is supported by Ebeling et al. (2021), who additionally found a dominant control of the vertical concentration gradient on the NO_3-N export dynamics in German catchments. Reduced riparian or instream NO_3-N removal during winter following the seasonal biogeochemical cycle (Lutz et al., 2020) could also enhance the pattern of synchronous *C* and *Q* seasonality.

2. The NO_3-N maximum coinciding with the *Q* minimum and vice versa (9.7% of the catchments, Figures 3a and S5) occurred in mountainous catchments, where asynchronous dilution patterns of *C-Q* dominate. Spring and summer discharge from mountains stemming from snow melt and summer precipitation could dilute N sources. In these archetypal catchments, mean NO_3-N concentrations are low (Figures 1c and 4a) due to relatively low N input in combination with strong dilution by high specific discharge (Figure 1b). The dominant dilution pattern agrees with *C-Q* relationships observed previously in mountainous, snow-dominated German meso-scale catchments (Ebeling et al., 2021). The dilution of N sources is lowest during LF season, that is late summer in southern France and autumn or winter in southern Germany. The dilution pattern of this archetype likely results from the spatial separation of discharge generating zones upstream and dominant agricultural sources downstream, potentially masking other export dynamics in the downstream areas.

3. NO_3-N maxima are reached during summer LF and minima mostly during autumn before the winter HF period (6.6% of the catchments, Figures 3a and S5). This type of NO_3-N seasonality with relatively weak dilution patterns, high mean concentrations and small relative seasonal differences between LF and HF concentration seems to be specific to the Armorican Massif and has been described for several catchments in this region previously (Abbott, Moatar, et al., 2018; Guillemot et al., 2021; Martin et al., 2004). The strong *Q* seasonality in that region and fast hydrological responses (e.g., high flashiness and CVQ) are not reflected in the NO_3-N seasonality, indicating a rather chemostatic export regime (low concentration relative to high *Q* variability) for this archetype. Reasons for this pattern include large legacy stores (Dupas et al., 2020) and bottom-loaded profiles with NO_3^--rich groundwater which is diluted during HF (Martin et al., 2006) in combination with potential bypassing of the riparian zones where removal by denitrification can be high during LF (Fovet et al., 2018). However, riparian zones can also act as NO_3^- sources during LF (Duncan et al., 2015), offering a nonexclusive alternative mechanism for this pattern. Van Meter et al. (2020) found that NO_3^--rich groundwater can lead to an out-of-phase or aseasonal NO_3^- pattern. In case of bottom-loaded profiles, we would expect the catchments to have developed the reverse seasonality over time, as described in for example Ehrhardt et al. (2019), which was indeed observed for some catchments (see Figure S6, crossing the 1:1 line). Alternatively, multiple contributing aquifers with variable response times and sources could be horizontally distributed differently with a longitudinal gradient, with a dominance of nonagricultural wetland soils upstream and agricultural areas downstream. With the upstream discharge diluting downstream sources during HF, this process resembles archetype 2. Another contributing mechanism to this pattern could be the seasonal variation of N inputs as fertilizer is primarily applied in spring or of retention in the soils.

4.2. Long-Term Trajectories of Nitrate Seasonality Integrate Complex Controls

We observed both long-term trajectory types equally often, with annual C_{LF} (counterclockwise hysteresis) or C_{HF} (clockwise hysteresis) changing first. Our hypothesis of dominant clockwise hysteresis for NO_3^- is therefore not supported by the studied catchments. Surprisingly, 20% of the catchments even switched their seasonal timing at least once during the observation period, which imposes substantial changes to aquatic

ecosystems over time. As described in the introduction, this could create shifts in nutrient availability and limitation during sensitive time periods for aquatic organisms and ecosystems (Minaudo et al., 2015).

The C_{HF} and C_{LF} are influenced by various controls that may lead to the observed long-term trajectories and hysteresis patterns. For example, in the densely populated Wupper catchment, changes in point sources could have affected C_{LF} more and earlier than C_{HF}, as discussed by Abbott, Moatar, et al. (2018). Reductions in inputs from point sources usually have a more immediate effect on riverine concentrations and have typically been achieved more easily and earlier than reductions in diffuse-source inputs in Western Europe (Le Moal et al., 2019; Westphal et al., 2020). The example catchments Leine and Rance (Figure 3c) are agriculturally managed with few point sources only and show the expected stronger delay in low-flow concentrations (clockwise hysteresis). This suggests that our hypothesis of changes in diffuse sources being reflected first in changes in C_{HF} may be supported for these two catchments but cannot be verified across the entire set of catchments.

Despite the large sample size and rich ancillary data on catchment characteristics, we did not detect fundamental or general controls on hysteresis patterns. Over the whole range of study catchments, the source descriptors (i.e., land cover, N surplus, point sources, population density) did not show consistent relationships with hysteresis. Small differences between the hysteresis classes were apparent in catchment properties describing the hydroclimate and soil data, though they had a relatively low explanatory power. This suggests overall complex controls on the long-term hysteresis patterns over the large extent of the study, with several interacting controls potentially determining the observed trajectories that will be addressed in the following.

The complexity in controls of responses across a wider range of catchments is in line with recent research on the diversity of nutrient retention capacity in various surface and subsurface catchment components (Frei et al., 2020; Kolbe et al., 2019). In particular, the high hydrochemical complexity of the subsurface in combination with relatively sparse subsurface data availability makes regional to continental predictions exceedingly uncertain (Aquilina et al., 2018; Jawitz et al., 2020; Marçais et al., 2018). Moreover, the subsurface reactivity can experience long-term changes if availability of electron donors and thus denitrification potential decreases (Bouwman et al., 2013). Because soil, vadose, and aquifer hydrology and biogeochemistry directly influence both hydrological time lags and active nutrient retention, better characterization of subsurface parameters should be a major research priority (Condon et al., 2020; Li et al., 2021).

The diversity of human activities can also obscure the linkage between catchment characteristics and nutrient dynamics. Catchments with anthropogenic impact often have both point and diffuse N sources, creating complex and time-variant interactions that are not captured by the catchment attributes taken into account here. For example, in diffuse-source-dominated catchments, smaller point sources could still have changed more than diffuse sources and vice versa, hampering predictability of hysteresis by catchment descriptors representing more the source strengths. Point sources could mask changes caused by diffuse source changes especially in larger, more populated catchments (Dupas et al., 2017).

Another unaccounted factor could be long-term changes in in-stream nutrient uptake processes. For example, an increasing C_{LF} while C_{HF} is already decreasing could result from reduced uptake rates during summer. Reduced algal biomass production could be caused by reductions in phosphorus and increasing limitations (Bowes et al., 2011; Minaudo et al., 2015). For example, in the Frome catchment, changes in in-stream processes were even considered to dominantly control changes in NO_3^- seasonal amplitude because concurrent seasonal changes of NO_3^- in groundwater boreholes were not observed (Bowes et al., 2011). Additionally, NO_3^- could be released to the stream by decomposition of biomass in winter and further affect seasonality (Bowes et al., 2011).

The tendency of clockwise catchments to have higher precipitation seasonality (P_SI, Figure 4b) and low evapotranspiration (PET_mm) could relate to their occurance in the Alps and the Armorican Massif (Figure 3b). Conversely, the high relative Q seasonality (rQseas) was common for catchments in northeastern France and the Armorican Massif. This might indicate that pronounced hydroclimatic variability in relatively wet catchments enhances HF concentrations to react faster, whereas high PET_mm links to dominant counterclockwise hysteresis in central and southern France, although this does not seem to be an overall dominant control as predictive power remained low.

Interestingly, we found distinct hysteresis patterns in the regions with asynchronous archetypal patterns of long-term average *C*-*Q* seasonality (16.2% of the catchments). For example, in southern France, the strong seasonal dilution pattern was mostly combined with counterclockwise hysteresis, whereas in the Alps and in the Armorican Massif, clockwise hysteresis dominated (Figure 3b). Dilution of downstream sources from upstream discharge generation in mountainous catchments could generally cause a stronger trend in less diluted low-flow concentration when sources change. However, these diluting effects interact with other mechanisms at downstream locations, for example mobilization processes. Possibly, in southern France, the upstream signal dominates, while in the Alps with smaller relative seasonal *Q* variations, downstream signals could dominate the overall trajectories, and leading to faster high-flow concentration responses. For the Armorican Massif, high-flow concentration responding first to changes in dominant diffuse N-input could cause the clockwise hysteresis patterns. This is supported by generally higher deep and lower shallow groundwater concentrations causing dilution patterns which could result from long-term N-inputs and large legacy stores (Dupas et al., 2020). On the other hand, within the dominant archetype of synchronous average *C*-*Q* seasonality, the heterogeneity in trajectories and controls was high and no dominant general pattern and control was detectable in this study (as discussed above).

In essence, the seasonality trajectory and its corresponding hysteresis integrate all the above mentioned processes. The missing dominance emphasizes that over the study domain multiple controls are relevant and hierarchies vary. Many settings can lead to the same response pattern and seasonality trajectory.

4.3. Spatial Variability Larger and Better Predictable Than Long-Term Temporal Variability of Nitrate Seasonality

Spatial variability of seasonality among the catchments is larger than the long-term temporal variability of most catchments, even when including significant trends in the logarithmic seasonal ratio. Although the number of significant long-term trends in the seasonal ratio $\log(C_{HF}/C_{LF})$ (76%) and hysteresis patterns (59%) reveal distinct changes in NO_3^- seasonality on multi-decadal time scales in the majority of catchments, inter-catchment variability across the study area largely exceeded the temporal variability within a catchment. Dupas et al. (2019) and Abbott, Gruau, et al. (2018) also report examples of higher spatial than temporal variability, resulting in spatial persistence, that is stable spatial patterns among catchments through time. These two studies, based on shorter periods of six (Dupas et al., 2019) and 12 years (Abbott, Gruau, et al., 2018), include mainly seasonal variations. Our finding thus extends the spatial persistence concept for NO_3^- seasonality to decadal trajectories across a wide range of Western European catchments.

At the same time, we can better explain the spatial variability of long-term average seasonality and *C*-*Q* dynamics among the catchments (Section 4.1). In contrast, the differences in trajectories resulting from different response times of low-flow and high-flow concentrations were only poorly predictable from the available data, and only small differences in catchment characteristics were apparent between the hysteresis classes (Section 4.2). This could be due to the fact that trajectories are affected by multiple controls with asynchronous source changes and seasonally variable responses, possibly masking each other. Further investigation may include temporarily variable catchment descriptors, such as long-term data on point source inputs, and time series of ecological in-stream metrics such as chlorophyll-a.

5. Conclusions

We characterized average long-term NO_3^--*Q* seasonalities and their trajectories from long-term time series in 290 French and German catchments covering a large variety in hydroclimate, topography, lithology and anthropogenic pressures. We implemented a novel hysteresis approach using low- and high-flow NO_3-N concentration trajectories. Our main findings are:

- We observed a widespread dominance of concurrent maxima of *Q* and NO_3-N in winter (84%), supporting our hypothesis. Deviations from this archetype of long-term average *C*-*Q* seasonality were linked to topography and hydroclimatic seasonality, and to source heterogeneity or lithology especially in the Armorican Massif
- Surprisingly, counterclockwise and clockwise hysteresis patterns of low-flow and high-flow NO_3-N concentrations occurred equally often, thus we had to reject our hypothesis about dominant occurrence of

faster response during high flow. We exemplarily showed that indeed counterclockwise hysteresis can be found in point source dominated and clockwise hysteresis in agricultural catchments. However, the lack of a consistent pattern in the French and German catchments suggests a high level of complexity and potential interactions in the controls over the wide range of catchments. These controls need to be further disentangled in a set of catchments with better known input time series. We point out that scarce data especially on point source loads (including their temporal evolution) is limiting the understanding of catchment functioning across a large sample. Therefore monitoring efforts and data use policies should be improved

- Overall, we found that spatial variability of long-term average *C-Q* seasonality between the catchments was larger and easier to predict than its long-term temporal evolution at a single station

Our large sample study has several implications for water quality management. The dominant spatial variability indicates that (a) uniform regulations may not be appropriate but need to take the spatial variability into account and should target the management regionally, and (b) short-term monitoring can already be useful to characterize the overall system functioning. The distinction between low- and high-flow trajectories can guide ecological assessment and water quality management considering that aquatic ecosystems are more prone to eutrophication during low flow, while exported loads are more susceptible to changes in high flows.

Conflict of Interest

The authors declare no conflicts of interest relevant to this study.

Data Availability Statement

Datasets used for this research are available at Ebeling and Dupas (2021), Musolff et al. (2020 original data in institutional repository), Musolff (2020), http://naiades.eaufrance.fr/ and http://hydro.eaufrance.fr/, Ehrhardt et al., 2021. References to further original datasets used for the catchment characteristics repository are given in the Table S1.

References

Abbott, B. W., Bishop, K., Zarnetske, J. P., Hannah, D. M., Frei, R. J., Minaudo, C., et al. (2019). A water cycle for the Anthropocene. *Hydrological Processes*, *33*(23), 3046–3052. https://doi.org/10.1002/hyp.13544

Abbott, B. W., Gruau, G., Zarnetske, J. P., Moatar, F., Barbe, L., Thomas, Z., et al. (2018). Unexpected spatial stability of water chemistry in headwater stream networks. *Ecology Letters*, *21*(2), 296–308. https://doi.org/10.1111/ele.12897

Abbott, B. W., Moatar, F., Gauthier, O., Fovet, O., Antoine, V., & Ragueneau, O. (2018). Trends and seasonality of river nutrients in agricultural catchments: 18 years of weekly citizen science in France. *Science of the Total Environment*, *624*, 845–858. https://doi.org/10.1016/j.scitotenv.2017.12.176

Altmann, A., Toloşi, L., Sander, O., & Lengauer, T. (2010). Permutation importance: A corrected feature importance measure. *Bioinformatics*, *26*(10), 1340–1347. https://doi.org/10.1093/bioinformatics/btq134

Aquilina, L., Roques, C., Boisson, A., Vergnaud-Ayraud, V., Labasque, T., Pauwels, H., et al. (2018). Autotrophic denitrification supported by biotite dissolution in crystalline aquifers (1): New insights from short-term batch experiments. *Science of the Total Environment*, *619*, 842–853. https://doi.org/10.1016/j.scitotenv.2017.11.079

Ascott, M. J., Gooddy, D. C., Wang, L., Stuart, M. E., Lewis, M. A., Ward, R. S., & Binley, A. M. (2017). Global patterns of nitrate storage in the vadose zone. *Nature Communications*, *8*(1), 1416. https://doi.org/10.1038/s41467-017-01321-w

Aubert, A. H., Gascuel-Odoux, C., Gruau, G., Akkal, N., Faucheux, M., Fauvel, Y., et al. (2013). Solute transport dynamics in small, shallow groundwater-dominated agricultural catchments: Insights from a high-frequency, multisolute 10 yr-long monitoring study. *Hydrology and Earth System Sciences*, *17*(4), 1379–1391. https://doi.org/10.5194/hess-17-1379-2013

Benettin, P., Bailey, S. W., Rinaldo, A., Likens, G. E., McGuire, K. J., & Botter, G. (2017). Young runoff fractions control streamwater age and solute concentration dynamics. *Hydrological Processes*, *31*(16), 2982–2986. https://doi.org/10.1002/hyp.11243

Benettin, P., Fovet, O., & Li, L. (2020). Nitrate removal and young stream water fractions at the catchment scale. *Hydrological Processes*, *34*(12), 2725–2738. https://doi.org/10.1002/hyp.13781

Berghuijs, W. R., Harrigan, S., Molnar, P., Slater, L. J., & Kirchner, J. W. (2019). The relative importance of different flood-generating mechanisms across Europe. *Water Resources Research*, *55*(6), 4582–4593. https://doi.org/10.1029/2019WR024841

Blaszczak, J. R., Delesantro, J. M., Urban, D. L., Doyle, M. W., & Bernhardt, E. S. (2019). Scoured or suffocated: Urban stream ecosystems oscillate between hydrologic and dissolved oxygen extremes. *Limnology and Oceanography*, *64*(3), 877–894. https://doi.org/10.1002/lno.11081

Blöschl, G., Hall, J., Parajka, J., Perdigão, R. A. P., Merz, B., Arheimer, B., et al. (2017). Changing climate shifts timing of European floods. *Science*, *357*(6351), 588–590. https://doi.org/10.1126/science.aan2506

Botter, M., Li, L., Hartmann, J., Burlando, P., & Fatichi, S. (2020). Depth of solute generation is a dominant control on concentration-discharge relations. *Water Resources Research*, *56*, e2019WR026695. https://doi.org/10.1029/2019WR026695

Bouraoui, F., & Grizzetti, B. (2011). Long term change of nutrient concentrations of rivers discharging in European seas. *Science of the Total Environment*, *409*(23), 4899–4916. https://doi.org/10.1016/j.scitotenv.2011.08.015

Bouwman, A. F., Bierkens, M. F. P., Griffioen, J., Hefting, M. M., Middelburg, J. J., Middelkoop, H., & Slomp, C. P. (2013). Nutrient dynamics, transfer and retention along the aquatic continuum from land to ocean: Towards integration of ecological and biogeochemical models. *Biogeosciences*, *10*(1), 1–22. https://doi.org/10.5194/bg-10-1-2013

Bowes, M. J., Smith, J. T., Neal, C., Leach, D. V., Scarlett, P. M., Wickham, H. D., et al. (2011). Changes in water quality of the River Frome (UK) from 1965 to 2009: Is phosphorus mitigation finally working? *Science of the Total Environment*, *409*(18), 3418–3430. https://doi.org/10.1016/j.scitotenv.2011.04.049

Casquin, A., Gu, S., Dupas, R., Petitjean, P., Gruau, G., & Durand, P. (2020). River network alteration of C-N-P dynamics in a mesoscale agricultural catchment. *Science of the Total Environment*, *749*, 141551. https://doi.org/10.1016/j.scitotenv.2020.141551

CLC. (2006). *CORINE land cover*. Retrieved from https://land.copernicus.eu/pan-european/corine-land-cover

Condon, L. E., Markovich, K. H., Kelleher, C. A., McDonnell, J. J., Ferguson, G., & McIntosh, J. C. (2020). Where is the bottom of a watershed? *Water Resources Research*, *56*(3), e2019WR026010. https://doi.org/10.1029/2019WR026010

Cornes, R. C., van der Schrier, G.,van den Besselaar, E. J. M., & Jones, P. D. (2018). An ensemble version of the E-OBS temperature and precipitation data sets. *Journal of Geophysical Research: Atmospheres*, *123*, 9391–9409. https://doi.org/10.1029/2017jd028200

Diaz, R. J., & Rosenberg, R. (2008). Spreading dead zones and consequences for marine ecosystems. *Science*, *321*(5891), 926–929. https://doi.org/10.1126/science.1156401

Duncan, J. M., Band, L. E., Groffman, P. M., & Bernhardt, E. S. (2015). Mechanisms driving the seasonality of catchment scale nitrate export: Evidence for riparian ecohydrologic controls. *Water Resources Research*, *51*, 3982–3997. https://doi.org/10.1002/2015WR016937

Dupas, R., Ehrhardt, S., Musolff, A., Fovet, O., & Durand, P. (2020). Long-term nitrogen retention and transit time distribution in agricultural catchments in western France. *Environmental Research Letters*, *15*(11), 115011. https://doi.org/10.1088/1748-9326/abbe47

Dupas, R., Jomaa, S., Musolff, A., Borchardt, D., & Rode, M. (2016). Disentangling the influence of hydroclimatic patterns and agricultural management on river nitrate dynamics from sub-hourly to decadal time scales. *Science of the Total Environment*, *571*, 791–800. https://doi.org/10.1016/j.scitotenv.2016.07.053

Dupas, R., Minaudo, C., & Abbott, B. W. (2019). Stability of spatial patterns in water chemistry across temperate ecoregions. *Environmental Research Letters*, *14*(7), 074015. https://doi.org/10.1088/1748-9326/ab24f4

Dupas, R., Minaudo, C., Gruau, G., Ruiz, L., & Gascuel-Odoux, C. (2018). Multidecadal trajectory of riverine nitrogen and phosphorus dynamics in rural catchments. *Water Resources Research*, *54*, 5327–5340. https://doi.org/10.1029/2018WR022905

Dupas, R., Musolff, A., Jawitz, J. W., Rao, P. S. C., Jäger, C. G., Fleckenstein, J. H., et al. (2017). Carbon and nutrient export regimes from headwater catchments to downstream reaches. *Biogeosciences*, *14*(18), 4391–4407. https://doi.org/10.5194/bg-14-4391-2017

Ebeling, P. (2021). *CCDB - Catchment characteristics database Germany, HydroShare*. [Dataset]. https://doi.org/10.4211/hs.0fc1b5b1be4a475aacfd9545e72e6839

Ebeling, P., & Dupas, R. (2021). *CCDB - Catchment characteristics data base France and Germany, HydroShare*. [Dataset]. https://doi.org/10.4211/hs.c7d4df3ba74647f0aa83ae92be2e294b

Ebeling, P., Kumar, R., Weber, M., Knoll, L., Fleckenstein, J. H., & Musolff, A. (2021). Archetypes and controls of riverine nutrient export across German catchments. *Water Research*. e2020WR028134. https://doi.org/10.1029/2020WR028134

EEA. (2013). *DEM over Europe from the GMES RDA project (EU-DEM, resolution 25m) - version 1*. Dataset.

EEC. (1991a). *Council Directive 91/271/EEC of 21 May 1991 concerning urban wastewater treatment*. European Economic Community.

EEC. (1991b). *Council Directive 91/676/EEC of 12 December 1991 concerning the protection of waters against pollution caused by nitrates from agricultural sources*. European Economic Community.

Ehrhardt, S., Ebeling, P., & Dupas, R. (2021). *Exported French water quality and quantity data, HydroShare*. [Dataset]. https://doi.org/10.4211/hs.d8c43e1e8a5a4872bc0b75a45f350f7a

Ehrhardt, S., Ebeling, P., Dupas, R., Kumar, R., Fleckenstein, J., & Musolff, A. (2020). Nitrate transport and retention in Western European catchments are shaped by hydroclimate and subsurface properties. *Earth and Space Science Open Archive*. https://doi.org/10.1002/essoar.10505117.4

Ehrhardt, S., Kumar, R., Fleckenstein, J. H., Attinger, S., & Musolff, A. (2019). Trajectories of nitrate input and output in three nested catchments along a land use gradient. *Hydrology and Earth System Sciences*, *23*(9), 3503–3524. https://doi.org/10.5194/hess-23-3503-2019

Fovet, O., Humbert, G., Dupas, R., Gascuel-Odoux, C., Gruau, G., Jaffrezic, A., et al. (2018). Seasonal variability of stream water quality response to storm events captured using high-frequency and multi-parameter data. *Journal of Hydrology*, *559*, 282–293. https://doi.org/10.1016/j.jhydrol.2018.02.040

Frei, R. J., Abbott, B. W., Dupas, R., Gu, S., Gruau, G., Thomas, Z., et al. (2020). Predicting nutrient incontinence in the Anthropocene at watershed scales. *Frontiers in Environmental Science*, *7*(200). https://doi.org/10.3389/fenvs.2019.00200

Gnann, S. J., Howden, N. J. K., & Woods, R. A. (2020). Hydrological signatures describing the translation of climate seasonality into streamflow seasonality. *Hydrology and Earth System Sciences*, *24*(2), 561–580. https://doi.org/10.5194/hess-24-561-2020

Godsey, S. E., Kirchner, J. W., & Clow, D. W. (2009). Concentration-discharge relationships reflect chemostatic characteristics of US catchments. *Hydrological Processes*, *23*(13), 1844–1864. https://doi.org/10.1002/hyp.7315

Guillemot, S., Fovet, O., Gascuel-Odoux, C., Gruau, G., Casquin, A., Curie, F., et al. (2021). Spatio-temporal controls of C–N–P dynamics across headwater catchments of a temperate agricultural region from public data analysis. *Hydrology and Earth System Sciences*, *25*(5), 2491–2511. https://doi.org/10.5194/hess-25-2491-2021

Gupta, H. V., Perrin, C., Bloschl, G., Montanari, A., Kumar, R., Clark, M., & Andreassian, V. (2014). Large-sample hydrology: A need to balance depth with breadth. *Hydrology and Earth System Sciences*, *18*(2), 463–477. https://doi.org/10.5194/hess-18-463-2014

Hamilton, S. K. (2012). Biogeochemical time lags may delay responses of streams to ecological restoration. *Freshwater Biology*, *57*(s1), 43–57. https://doi.org/10.1111/j.1365-2427.2011.02685.x

Hirsch, R. M., & De Cicco, L. A. (2015). User Guide to Exploration and Graphics for RivEr Trends (EGRET) and dataRetrieval: R Packages for Hydrologic Data. *U.S. Geological Survey Techniques and Methods Book 4*, *4*. Chap. A10, 93. https://doi.org/10.3133/tm4A10

Hirsch, R. M., Moyer, D. L., & Archfield, S. A. (2010). Weighted Regressions on time, discharge, and season (WRTDS), with an application to Chesapeake Bay river inputs. *JAWRA Journal of the American Water Resources Association*, *46*(5), 857–880. https://doi.org/10.1111/j.1752-1688.2010.00482.x

Howden, N. J. K., Burt, T. P., Worrall, F., Whelan, M. J., & Bieroza, M. Z. (2010). Nitrate concentrations and fluxes in the River Thames over 140 years (1868–2008): Are increases irreversible? *Hydrological Processes*, *24*(18), 2657–2662. https://doi.org/10.1002/hyp.7835

Jawitz, J. W., Desormeaux, A. M., Annable, M. D., Borchardt, D., & Dobberfuhl, D. (2020). Disaggregating landscape-scale nitrogen attenuation along hydrological flow paths. *Journal of Geophysical Research: Biogeosciences*, 125, e2019JG005229. https://doi.org/10.1029/2019JG005229

Kolbe, T., de Dreuzy, J.-R., Abbott, B. W., Aquilina, L., Babey, T., Green, C. T., et al. (2019). Stratification of reactivity determines nitrate removal in groundwater. *Proceedings of the National Academy of Sciences*, 116(7), 2494–2499. https://doi.org/10.1073/pnas.1816892116

Kolbe, T., Marçais, J., Thomas, Z., Abbott, B. W., de Dreuzy, J.-R., Rousseau-Gueutin, P., et al. (2016). Coupling 3D groundwater modeling with CFC-based age dating to classify local groundwater circulation in an unconfined crystalline aquifer. *Journal of Hydrology*, 543, 31–46. https://doi.org/10.1016/j.jhydrol.2016.05.020

Krueger, T., Quinton, J. N., Freer, J., Macleod, C. J. A., Bilotta, G. S., Brazier, R. E., et al. (2009). Uncertainties in data and models to describe event dynamics of agricultural sediment and phosphorus transfer. *Journal of Environmental Quality*, 38(3), 1137–1148. https://doi.org/10.2134/jeq2008.0179

Kuentz, A., Arheimer, B., Hundecha, Y., & Wagener, T. (2017). Understanding hydrologic variability across Europe through catchment classification. *Hydrology and Earth System Sciences*, 21(6), 2863–2879. https://doi.org/10.5194/hess-21-2863-2017

Kumar, R., Heße, F., Rao, P. S. C., Musolff, A., Jawitz, J. W., Sarrazin, F., et al. (2020). Strong hydroclimatic controls on vulnerability to subsurface nitrate contamination across Europe. *Nature Communications*, 11(1), 6302. https://doi.org/10.1038/s41467-020-19955-8

Kumar, R., Samaniego, L., & Attinger, S. (2013). Implications of distributed hydrologic model parameterization on water fluxes at multiple scales and locations. *Water Resources Research*, 49(1), 360–379. https://doi.org/10.1029/2012wr012195

Lang, M., Binder, M., Richter, J., Schratz, P., Pfisterer, F., Coors, S., et al. (2019). MLR3: A modern object-oriented machine learning framework in R. *Journal of Open Source Software*, 4, 1903. https://doi.org/10.21105/joss.01903

Le Moal, M., Gascuel-Odoux, C., Ménesguen, A., Souchon, Y., Étrillard, C., Levain, A., et al. (2019). Eutrophication: A new wine in an old bottle? *Science of the Total Environment*, 651, 1–11. https://doi.org/10.1016/j.scitotenv.2018.09.139

Li, L., Sullivan, P. L., Benettin, P., Cirpka, O. A., Bishop, K., Brantley, S. L., et al. (2021). Toward catchment hydro-biogeochemical theories. *WIREs Water*, 8(1), e1495. https://doi.org/10.1002/wat2.1495

Lloyd, C. E. M., Freer, J. E., Johnes, P. J., & Collins, A. L. (2016). Technical Note: Testing an improved index for analysing storm discharge–concentration hysteresis. *Hydrology and Earth System Sciences*, 20(2), 625–632. https://doi.org/10.5194/hess-20-625-2016

Lutz, S. R., Trauth, N., Musolff, A., Van Breukelen, B. M., Knöller, K., & Fleckenstein, J. H. (2020). How important is denitrification in riparian zones? Combining end-member mixing and isotope modeling to quantify nitrate removal from riparian groundwater. *Water Resources Research*, 56, e2019WR025528. https://doi.org/10.1029/2019wr025528

Marçais, J., Gauvain, A., Labasque, T., Abbott, B. W., Pinay, G., Aquilina, L., et al. (2018). Dating groundwater with dissolved silica and CFC concentrations in crystalline aquifers. *Science of the Total Environment*, 636, 260–272. https://doi.org/10.1016/j.scitotenv.2018.04.196

Martin, C., Aquilina, L., Gascuel-Odoux, C., Molénat, J., Faucheux, M., & Ruiz, L. (2004). Seasonal and interannual variations of nitrate and chloride in stream waters related to spatial and temporal patterns of groundwater concentrations in agricultural catchments. *Hydrological Processes*, 18(7), 1237–1254. https://doi.org/10.1002/hyp.1395

Martin, C., Molénat, J., Gascuel-Odoux, C., Vouillamoz, J. M., Robain, H., Ruiz, L., et al. (2006). Modelling the effect of physical and chemical characteristics of shallow aquifers on water and nitrate transport in small agricultural catchments. *Journal of Hydrology*, 326(1), 25–42. https://doi.org/10.1016/j.jhydrol.2005.10.040

Meals, D. W., Dressing, S. A., & Davenport, T. E. (2010). Lag time in water quality response to best management practices: A review. *Journal of Environmental Quality*, 39(1), 85–96. https://doi.org/10.2134/jeq2009.0108

Minaudo, C., Abonyi, A., Leitão, M., Lançon, A. M., Floury, M., Descy, J.-P., & Moatar, F. (2020). Long-term impacts of nutrient control, climate change, and invasive clams on phytoplankton and cyanobacteria biomass in a large temperate river. *Science of the Total Environment*. https://doi.org/10.1016/j.scitotenv.2020.144074

Minaudo, C., Dupas, R., Gascuel-Odoux, C., Roubeix, V., Danis, P.-A., & Moatar, F. (2019). Seasonal and event-based concentration-discharge relationships to identify catchment controls on nutrient export regimes. *Advances in Water Resources*, 131, 103379. https://doi.org/10.1016/j.advwatres.2019.103379

Minaudo, C., Meybeck, M., Moatar, F., Gassama, N., & Curie, F. (2015). Eutrophication mitigation in rivers: 30 years of trends in spatial and seasonal patterns of biogeochemistry of the Loire River (1980–2012). *Biogeosciences*, 12(8), 2549–2563. https://doi.org/10.5194/bg-12-2549-2015

Moatar, F., Abbott, B. W., Minaudo, C., Curie, F., & Pinay, G. (2017). Elemental properties, hydrology, and biology interact to shape concentration-discharge curves for carbon, nutrients, sediment, and major ions. *Water Resources Research*, 53, 1270–1287. https://doi.org/10.1002/2016wr019635

Musolff, A. (2020). WQQDB - Water quality and quantity data base Germany: Metadata. *HydroShare*. Dataset. https://doi.org/10.4211/hs.a42addcbd59a466a9aa56472dfef8721

Musolff, A., Grau, T., Weber, M., Ebeling, P., Samaniego-Eguiguren, L., & Kumar, R. (2020). *WQQDB: Water quality and quantity data base Germany*. Dataset. Retrieved from http://www.ufz.de/record/dmp/archive/7754

Musolff, A., Schmidt, C., Rode, M., Lischeid, G., Weise, S. M., & Fleckenstein, J. H. (2016). Groundwater head controls nitrate export from an agricultural lowland catchment. *Advances in Water Resources*, 96, 95–107. https://doi.org/10.1016/j.advwatres.2016.07.003

Musolff, A., Schmidt, C., Selle, B., & Fleckenstein, J. H. (2015). Catchment controls on solute export. *Advances in Water Resources*, 86, 133–146. https://doi.org/10.1016/j.advwatres.2015.09.026

Newcomer, M. E., Bouskill, N. J., Wainwright, H., Maavara, T., Arora, B., Siirila-Woodburn, E. R., et al. (2021). Hysteresis patterns of watershed nitrogen retention and loss over the Past 50 years in United States hydrological basins. *Global Biogeochemical Cycles*, 35(4), e2020GB006777. https://doi.org/10.1029/2020GB006777

Raymond, P. A., Saiers, J. E., & Sobczak, W. V. (2016). Hydrological and biogeochemical controls on watershed dissolved organic matter transport: Pulse-shunt concept. *Ecology*, 97(1), 5–16. https://doi.org/10.1890/14-1684.1

Samaniego, L., Kumar, R., & Attinger, S. (2010). Multiscale parameter regionalization of a grid-based hydrologic model at the mesoscale. *Water Resources Research*, 46. https://doi.org/10.1029/2008WR007327

Sebilo, M., Mayer, B., Nicolardot, B., Pinay, G., & Mariotti, A. (2013). Long-term fate of nitrate fertilizer in agricultural soils. *Proceedings of the National Academy of Sciences*, 110(45), 18185–18189. https://doi.org/10.1073/pnas.1305372110

Seibert, J., Grabs, T., Köhler, S., Laudon, H., Winterdahl, M., & Bishop, K. (2009). Linking soil- and stream-water chemistry based on a riparian flow-concentration integration model. *Hydrology and Earth System Sciences*, 13(12), 2287–2297. https://doi.org/10.5194/hess-13-2287-2009

Sen, P. K. (1968). Estimates of the regression coefficient based on Kendall's Tau. *Journal of the American Statistical Association*, 63(324), 1379–1389. https://doi.org/10.1080/01621459.1968.10480934

Steffen, W., Richardson, K., Rockstrom, J., Cornell, S. E., Fetzer, I., Bennett, E. M., et al. (2015). Sustainability. Planetary boundaries: Guiding human development on a changing planet. *Science*, *347*(6223), 1259855. https://doi.org/10.1126/science.1259855

Van Meter, K. J., & Basu, N. B. (2015). Catchment legacies and time lags: A parsimonious watershed model to predict the effects of legacy storage on nitrogen export. *PloS One*, *10*(5), e0125971. https://doi.org/10.1371/journal.pone.0125971

Van Meter, K. J., & Basu, N. B. (2017). Time lags in watershed-scale nutrient transport: An exploration of dominant controls. *Environmental Research Letters*, *12*(8), 084017. https://doi.org/10.1088/1748-9326/aa7bf4

Van Meter, K. J., Basu, N. B., Veenstra, J. J., & Burras, C. L. (2016). The nitrogen legacy: Emerging evidence of nitrogen accumulation in anthropogenic landscapes. *Environmental Research Letters*, *11*(3), 035014. https://doi.org/10.1088/1748-9326/11/3/035014

Van Meter, K. J., Chowdhury, S., Byrnes, D. K., & Basu, N. B. (2020). Biogeochemical asynchrony: Ecosystem drivers of seasonal concentration regimes across the Great Lakes Basin. *Limnology and Oceanography*, *65*(4), 848–862. https://doi.org/10.1002/lno.11353

Vitousek, P. M., Mooney, H. A., Lubchenco, J., & Melillo, J. M. (1997). Human Domination of Earth's Ecosystems. *Science*, *277*(5325), 494–499. https://doi.org/10.1126/science.277.5325.494

Wang, L., Stuart, M. E., Lewis, M. A., Ward, R. S., Skirvin, D., Naden, P. S., et al. (2016). The changing trend in nitrate concentrations in major aquifers due to historical nitrate loading from agricultural land across England and Wales from 1925 to 2150. *Science of the Total Environment*, *542*(Pt), 694–705. https://doi.org/10.1016/j.scitotenv.2015.10.127

Westphal, K., Andreas, M., Daniel, G., & Dietrich, B. (2020). Controls of point and diffuse sources lowered riverine nutrient concentrations asynchronously, thereby warping molar N:P ratios. *Environmental Research Letters*. Retrieved from http://iopscience.iop.org/10.1088/1748-9326/ab98b6

Winter, C., Lutz, S. R., Musolff, A., Kumar, R., Weber, M., & Fleckenstein, J. H. (2020). Disentangling the impact of catchment heterogeneity on nitrate export dynamics from event to long-term time scales*n/a*(n/a). *Water Resources Research*, e2020WR027992. https://doi.org/10.1029/2020WR027992

Withers, P. J. A., & Jarvie, H. P. (2008). Delivery and cycling of phosphorus in rivers: A review. *Science of the Total Environment*, *400*(1), 379–395. https://doi.org/10.1016/j.scitotenv.2008.08.002

Wollheim, W. M., Mulukutla, G. K., Cook, C., & Carey, R. O. (2017). Aquatic nitrate retention at river network scales across flow conditions determined using nested in situ sensors. *Water Resources Research*, *53*, 9740–9756. https://doi.org/10.1002/2017wr020644

Wright, M. N., & Ziegler, A. (2017). Ranger: A fast implementation of random forests for high dimensional data in C++ and R. *Journal of Statistical Software*, *77*(1), 17. https://doi.org/10.18637/jss.v077.i01

Yang, J., Heidbüchel, I., Musolff, A., Reinstorf, F., & Fleckenstein, J. H. (2018). Exploring the dynamics of transit times and subsurface mixing in a small agricultural catchment. *Water Resources Research*, *54*, 2317–2335. https://doi.org/10.1002/2017WR021896

Zarnetske, J. P., Bouda, M., Abbott, B. W., Saiers, J., & Raymond, P. A. (2018). Generality of hydrologic transport limitation of watershed organic carbon flux across ecoregions of the United States. *Geophysical Research Letters*, *45*, 11702–11711. https://doi.org/10.1029/2018gl080005

Zhi, W., & Li, L. (2020). The shallow and deep hypothesis: Subsurface vertical chemical contrasts shape nitrate export patterns from different land uses. *Environmental Science & Technology*, *54*, 11915–11928. https://doi.org/10.1021/acs.est.0c01340